Rolling contact fatigue resistance of Carbidic Austempered Ductile Iron (CADI)

D.I. Pedro, R.C. Dommarco

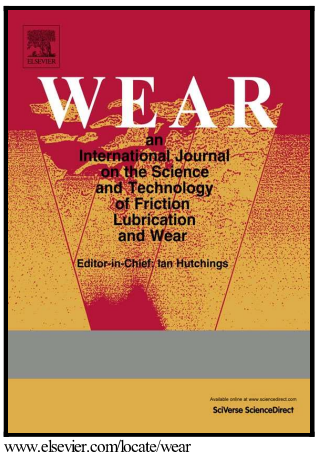

www.elsevier.com/locate/wear

PII: S0043-1648(18)30267-9
DOI: https://doi.org/10.1016/j.wear.2018.11.005
Reference: WEA102540

To appear in: *Wear*

Received date: 28 February 2018
Revised date: 2 November 2018
Accepted date: 8 November 2018

Cite this article as: D.I. Pedro and R.C. Dommarco, Rolling contact fatigue resistance of Carbidic Austempered Ductile Iron (CADI), *Wear,* https://doi.org/10.1016/j.wear.2018.11.005

Rolling contact fatigue resistance of Carbidic Austempered Ductile Iron (CADI)

D.I. Pedro*, R.C. Dommarco

INTEMA - CONICET/UNMDP
Av. Colón 10850, B7606BWV Mar del Plata, Argentina
** E-mail: dpedro@fi.mdp.edu.ar*

Abstract

The austempered ductile iron (ADI) with carbides in its microstructure, commonly known as CADI, is a relatively new variant of ductile iron intended to resist abrasive wear in different tribosystems by selecting the appropriate casting procedure, chemical composition and heat treatment.

In this case, the rolling contact fatigue (RCF) behavior of CADI with two heat treatments was compared to that of ADI to evaluate its potential use as an alternative material for machine parts subjected to point or line rolling/sliding contact fatigue conditions.

The RCF tests were done in a flat washer type testing machine under contact conditions (load, roughness, lubricant and velocity) leading to contact of micro-asperities.

When compared to ADI, the microstructure of CADI has similar nodularity and nodule size, but the nodule count is lower because part of the carbon is combined in the form of carbides. While having similar hardness and failure appearance, CADI RCF resistance was higher than that of ADI. It was observed that the nodules at or near the surface work as crack nucleation sites and then, when replacing part of the graphite content with carbides the load carrying capacity and the RCF resistance are improved with respect to those of ADI.

Keywords: CADI, ADI, RCF, CARBIDE, GRAPHITE, ASPERITY CONTACT

1 Introduction

Ductile Iron (DI) family has evolved since its introduction in the market during the 1950´s. An iconic variant of this family is the Austempered Ductile Iron (ADI) introduced in the 1970´s, with such interesting mechanical properties that helped to expand its application around the world, replacing forged or cast steels in many applications. Thanks to its particular microstructure with a matrix composed by a fine mixture of ferrite and austenite called ausferrite, ADI is able to reach very high tensile strength and very good toughness (over 100 J and over 1600 MPa for grades 1 and 5, respectively, according to the ASTM A834-95).

When looking to applications that require high wear resistance, DI and particularly ADI should also be considered because those materials may adapt to the different wear mechanisms (abrasion, adhesion, contact fatigue, tribo-corrosion) by controlling its particular microstructure [1, 2]. Typical applications of those materials are those that require good tensile strength and toughness, frequently combined with good wear resistance as for example in gears, cams and followers, and parts exposed

to severe abrasive and erosive conditions as those encountered in agriculture and the mining industries.

Between others, a further development of DI in the 1990´s considered the introduction of carbides in the ADI microstructure with the intention to reinforce the matrix when subjected to abrasive wear. This new DI variant was called Carbidic Austempered Ductile Iron (CADI). In many tribosystems the incorporation of hard particles enhances the abrasion resistance but reduces the impact toughness [3]. However, CADI has higher impact toughness than other materials with similar abrasion resistance at lower production cost [4]. It also has higher added value than other DI variants and requires near zero investment to incorporate it as a new product line in an existing facility.

Until now, CADI research work was much related to its application as an abrasion resistant material. In this case, the CADI Rolling Contact Fatigue (RCF) resistance is evaluated studying the relationship between performance and microstructure, determining those microstructural characteristics that could be controlled in order to optimize the RCF resistance.

At first sight the RCF behavior depends on material hardness, which can be controlled by carbide content, ausferritic matrix properties (retained austenite volume and carbon content), nodule count, etc. These microstructural characteristics can be controlled by the chemical composition, mold design, heat treatment, etc. In the present work, Cr alloyed carbidic or mottled ductile iron was cast in the form of plates from which the RCF samples in the form of disks were machined and then heat treated by austempering in order to obtain the CADI RCF samples to be tested in a flat washer type testing machine.

2 Experimental procedures

2.1 Materials and sample preparation

Ductile Iron (DI) and Mottled Ductile Iron (MDI) used in this paper were cast in a 1500 kg induction furnace with network frequency (50 Hz). FeSi and FeSiMg were used for inoculation and nodulization, respectively, in a ladle with nodulization pocket. Cast pieces consist of flat plates of (250x250x13) mm.

Base material chemical composition was analyzed by optical emission spectrometry and the reported values in Table 1 are the average of four measurements on each material.

Table 1: Chemical composition of DI and MDI (wt %).

Identif.	Fe	C	Si	Mn	S	P	Mg	Ni	Mo	Cu	Cr	CE
DI	Bal.	3,43	2,68	0,5	<0,04	<0,04	0,05	0,62	0,44	0,97	-	4,26
MDI	Bal.	3,66	3,01	0,42	<0,02	<0,04	<0,02	0,239	0,313	0,875	1,53	4,5

The RCF samples were machined from the cast plates into disks with a centered thread for mounting purposes, final dimensions of the samples were 62 mm outer diameter and 10 mm thick, Fig. 1. Afterwards, samples were heat treated by austempering, consisting of an austenitizing step at $T\gamma$=910 °C for $t\gamma$=120 min and then an austempering in a salt bath at Ta=280 °C for DI and MDI and at Ta=360 °C

for MDI, with subsequent air cooling to room temperature in all cases. The identification of the samples is listed in Table 2.

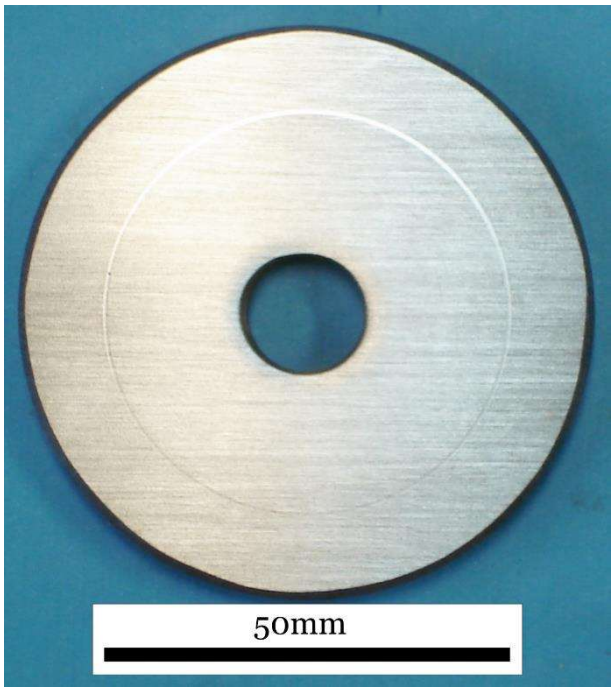

Fig. 1: RCF Flat washer sample with rolling track.

Table 2: Sample identification, base material and heat treatment parameters.

Identif.	Material	Tγ - °C	tγ - min	Ta - °C	ta - min
ADI280	DI	910	90	280	90
CADI280	MDI	910	90	280	90
CADI360	MDI	910	90	360	90

2.2 Samples surface finishing

Heat treated samples were finished with a vertical spindle surface grinder to remove any surface influence of heat treatment (oxidation, decarburization). Afterwards, in order to control surface roughness, the samples were manually sanded with 100 grit size SiC waterproof sand paper.

The samples roughness was measured with a Taylor Hobson Surtronic 3+ with a 2 µm radius tip diamond stylus and a cut-off of 0.8 mm. The average roughness (Ra or CLA) and its standard deviation from 6 measurements are summarized in Table 3.

Table 3: Surface roughness characteristics for RCF samples.

Identif.	Ra - µm	Std. Dev. - µm
ADI280	0.31	0.02
CADI360	0.31	0.05
CADI280	0.32	0.02

2.3 Materials Characterization

The carbide and graphite contents (% vol) and the nodule count were measured by optical microscopy and digital image analysis. Carbides were revealed by etching 2 min with a water solution of ammonium persulfate (10 % vol). The microstructure was evaluated in the as cast and the heat-treated conditions at the RCF samples surface.

The phases of the matrix after heat treatment were quantified by X-ray diffraction (XRD) measurements using a Panalytical X'pert Pro operating with a copper anode (Kα=1.542 Å) at 40 kV / 40 mA and 240 mm goniometer radius and graphite monochromator for Kβ filtration. A divergence slit of 1° was used with a 0.1 mm receiving slit. Samples were scanned from 20 to 120° of 2θ with 0.02° steps (Δ2θ) and counting time of 4.5 s. Austenite and ferrite contents were measured by XRD pattern analysis [5] and the relative volume fraction was determined using the ratio between integrated intensity from at least 3 diffraction peaks from each phase and theoretical references, then corrected taking into account the volume fraction of carbide and graphite not determined by XRD.

The bulk hardness was measured by using the Rockwell method in the C scale (HRC) while the hardness of the matrix was measured by micro-indentation test using the Vickers method and a 300 g load (HV_{300}). At least 6 measures were taken from the heat-treated samples and the average and standard deviation are reported.

Instrumented nano indentation tests were also carried out to characterize hardness (H) and Young's modulus (Er) of the different phases by the Oliver-Parr method [6]. A Triboindenter Hysitron with the MRNP module according to ISO 14577-1 standard was used. Due to the small size of each phase the maximum load was 165 mN for carbides and metallic matrix and 2 mN for graphite in order to limit indentation size to 5 µm side (750 nm depth). A 5 s ramp was used on loading and unloading with a holding time of 2 s. At least 6 measures were taken for carbide and graphite and at least 6 indentation grids were taken on the metallic matrix. Tests were analyzed according to adequate indenter area compensation.

2.4 RCF tests

The RCF tests were performed in a flat washer axial thrust machine type, Fig. 2. In this test rig, a sample disk (1) is loaded against the balls of a thrust ball bearing of the type 51107 (2) at a fixed angular speed under lubricated pure rolling conditions. The sample was rotated at 1748 rpm resulting in 1.1 million cycles per hour. The load was selected after several preliminary tests focused on maximizing the load, thus minimizing test duration, but avoiding generalized plastic strain. For the applied load (3 kgf per bearing ball) the elastic theory determines the maximum contact pressure p_o = 1800 MPa and a rolling track width 2a = 170 µm. An ISO VG 100 oil was used with magnetic filtration. The specific oil film thickness parameter (λ) can be calculated by the ratio between the minimum oil film thickness (h_o) and the composite surface roughness (Ra_c). The contact conditions were set for asperity interaction $\lambda < 2$. The h_o value was calculated using the Hamrock and Dowson equation [7] and the resulting h_o=0.6 µm combined with the Ra values in Table 3 lead to $1.83 < \lambda < 1.91$.

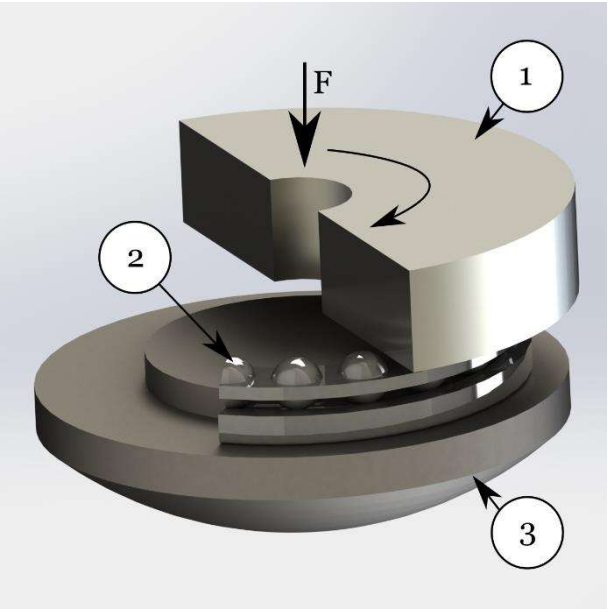

Fig. 2: RCF test setup, the sample (1) is pressed against the balls (counter-sample) from a 51107 bearing (2) fixed on top of an universal spherical joint (3) at a fixed angular speed.

Each RCF test was run until a spall or crater was produced on the rolling track and this event was detected by an accelerometer that stopped the machine immediately. The test duration until failure (then converted into loading cycles) was measured by a time counter. A minimum of 6 tests were carried out for each sample group or material variant. Fatigue life ranks were calculated using median and fit with a two parameter Weibull with rank regression, x on y. This method is appropriate to fit a reduced population (2-100 points). The parameter R^2 calculated from the curve fitted Weibull distributions shows good fits ($R > 0.92$).

Rolling tracks of the samples were verified with a stylus profilometer. Failures were carefully examined by optical microscopy.

3 Results and discussion

3.1 Metallographic characterization

The as cast DI microstructure consisted in graphite nodules immersed in a matrix composed by free ferrite and a majority of pearlite, as shown in Fig. 3. According to the ASTM A247 standard the nodularity exceeded 80 %, the nodule count (NC) was 320 nod/mm² and an average nodule size (NS) of 18 µm (matches N°6, ASTM A247). Measured by image analysis on unetched samples the graphite content was about 8.6 % vol.

In Fig. 4, the as cast MDI structure is shown. The matrix was fully pearlitic and finner than that of DI. The nodularity was higher than 80 %, the NC was 193 nod/mm² and a NS of 21 µm (matches N°6, ASTM A247). The graphite content was 6.1 %. In Fig. 5, the etching with ammonium persulfate allows to clearly distinguish carbides with respect to the rest of the phases, facilitating the image analysis measurements. The carbide content of MDI was about 6.4 % vol.

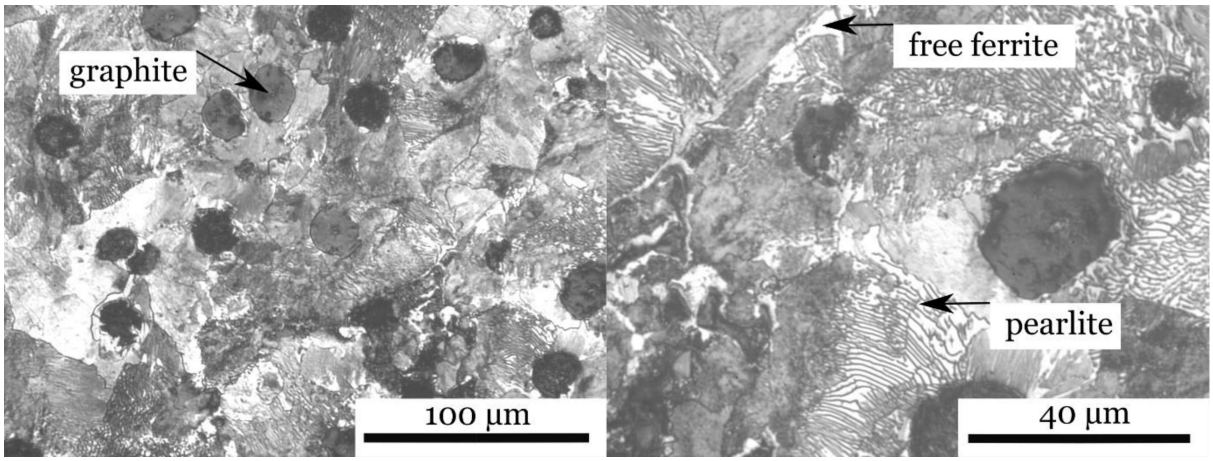

Fig. 3: The DI microstructure in the as cast condition presents spherical graphite immersed in a metallic matrix mainly composed of fine pearlite with some traces of free ferrite. Nital 2 % etch.

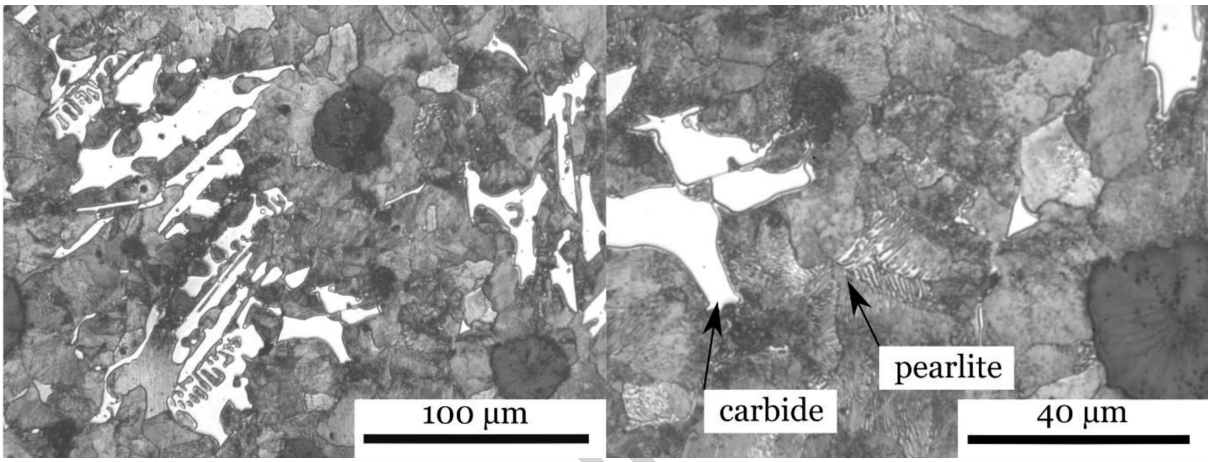

Fig. 4: The MDI microstructure in the as cast condition presents spherical graphite and bulk carbides immersed in a pearlitic matrix. Nital 2 % etch.

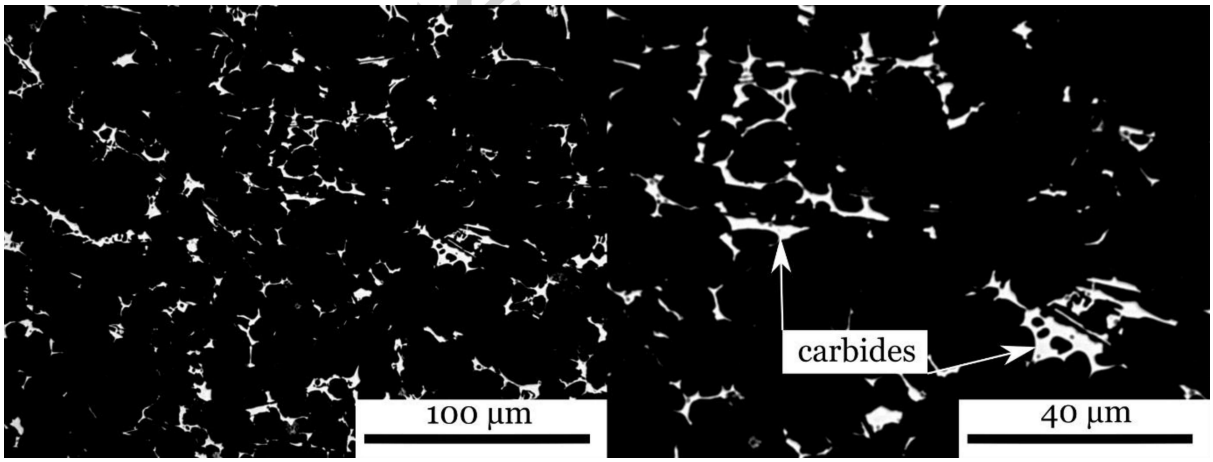

Fig. 5: Etching CADI with the ammonium persulfate water solution (10 %) reveals the carbides (white regions) with high contrast.

As shown in Fig. 6, the ADI280 microstructure consists of graphite nodules immersed in an acicular ausferrite, characteristic of the applied austempering temperature.

The microstructures of MDI converted into CADI360 and CADI280 after austempering are shown in Fig. 7 and Fig. 8. Graphite nodules remained intact and carbides were not dissolved by heat treatment due to the stabilization provided by the alloying elements [3]. Depending on the austempering temperature (Ta) the remaining microstructure transformed into a feathery ausferrite in the CADI360 (typical of the upper bainite) Fig. 7, and into an acicular ausferrite in the CADI280 (typical of the lower bainite) Fig. 8, as also seen in ADI280, Fig. 6.

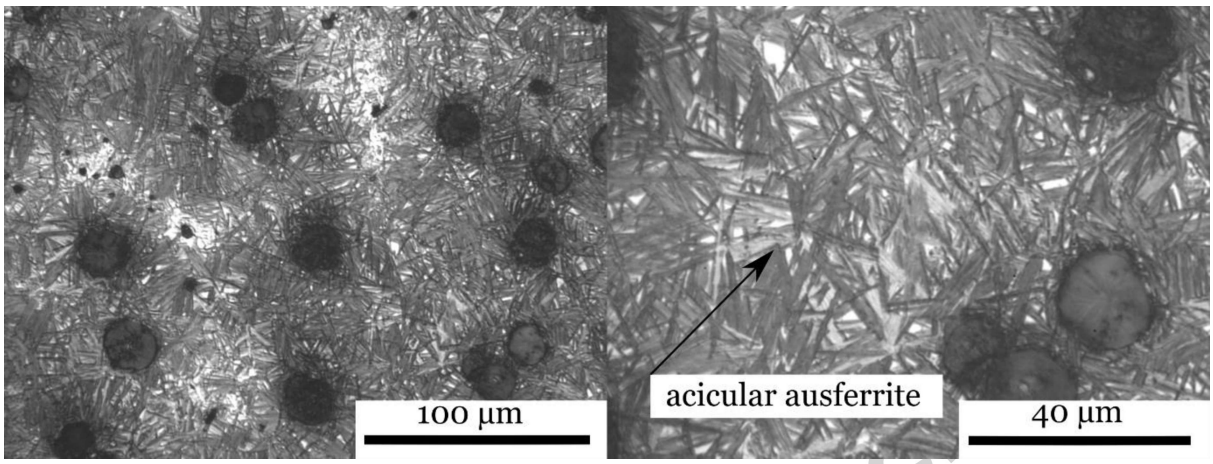

Fig. 6: The austempering heat treatment of DI with a salt bath temperature of 280 °C results in the ADI280 microstructure showing spherical graphite immersed in acicular ausferrite. Nital 2 %.

The phases of the samples were quantified by a combination of optical microscopy processed by image analysis and X-ray diffraction measurements, Fig. 9. The XRD results were corrected by the carbide and graphite content measured by image analysis with the results listed in Table 4. The retained austenite content was maximum for the CADI360 (50.1 %) followed by the CADI280 (37 %) and the minimum was measured for the ADI280 (27.1 %). The difference of austenite content between CADI360 and CADI280 results from the two different salt bath temperatures. At the lower temperature heat treatment, Ta=280 °C, ferrite is forced to transform into many needles because of the low carbon diffusion compensated by a high nucleation rate, which results in a low content of high carbon retained austenite. However, the difference between the austenite content of CADI280 and ADI280 is related with the different chemical composition of the metallic matrix, i.e. not all the chromium content forms carbides. The difference between matrix alloying elements changes the conditions for the solid-state transformation leading to some differences in the kinetics and resulting phase contents. All the heat-treated structures shown in Fig. 6 to Fig. 8 are consistent with the quantification results.

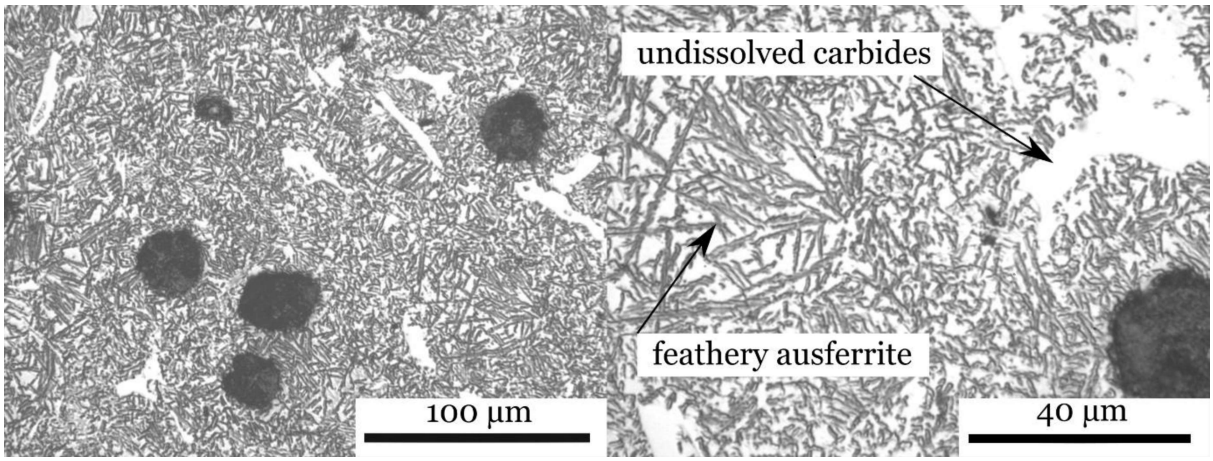

Fig. 7: The austempering heat treatment of MDI at a salt bath temperature of 360 °C results in the CADI360 microstructure showing unchanged carbides and spherical graphite immersed in an upper ausferrite (feathery) metallic matrix. Nital 2 %.

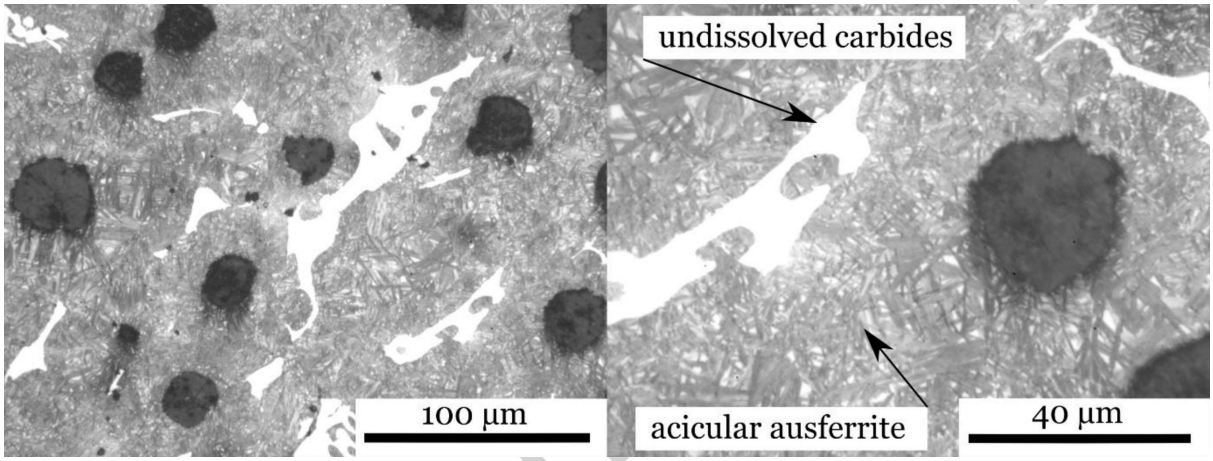

Fig. 8: The austempering heat treatment of MDI with a salt bath temperature of 280 °C results in the CADI280 microstructure showing unchanged carbides and spherical graphite immersed in an acicular ausferrite mettalic matrix. Nital 2 %.

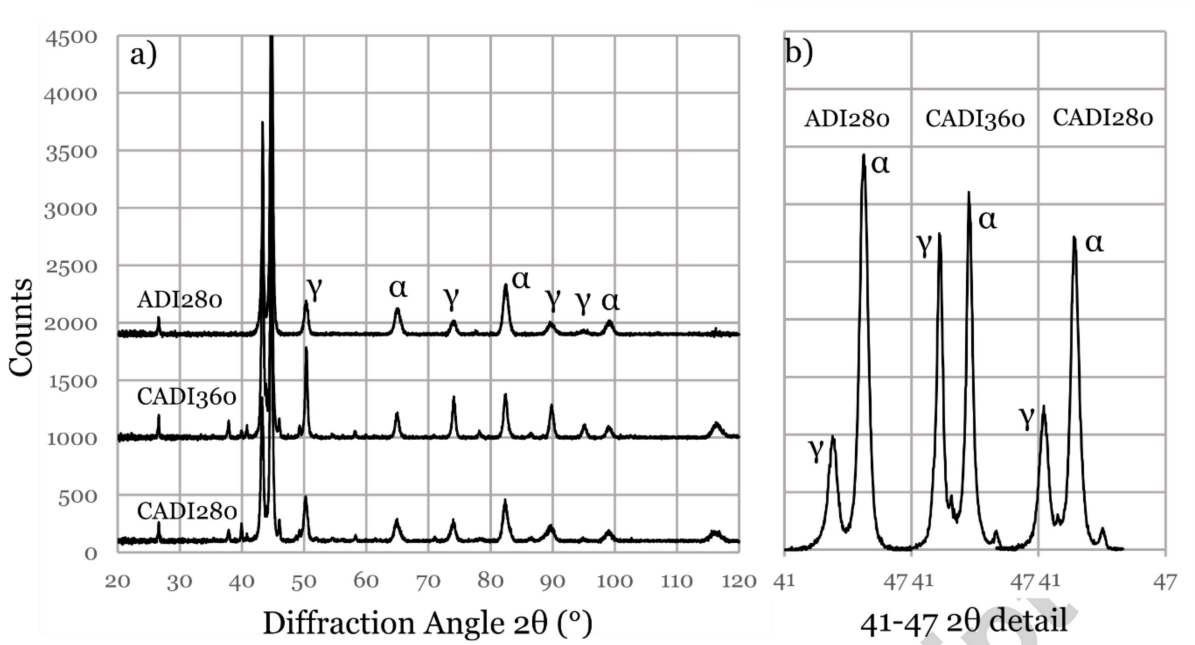

Fig. 9: XRD pattern a) full pattern b) highest peaks detail (2θ=41-47°). The difference in austenite content is clearly visible where CADI360 has the highest and ADI280 the lowest.

Table 4: Phases amount by quantitative metallography and XRD analysis (% vol).

Identif.	Graphite - %	Carbides - %	Austenite - %	Ferrite - %
ADI280	8.8	0.0	27.1	64.1
CADI360	6.1	6.4	50.1	37.4
CADI280	6.1	6.4	37.0	50.5

Elastic properties and hardness at the nano scale were measured for the different phases and are reported in Table 5. The measurement of the Young´s modulus of elasticity shows similar values for the different matrices and also for carbides, while that of graphite was found to be about five times lower. The bulk hardness and the hardness of the different phases were measured by hardness and micro indentation tests, respectively, as listed in Table 6. Carbide hardness at the micro scale was not measured. Even though hardness and nano hardness results are not comparable, the order and relative values was similar for both methods, being the nano scale measurements higher.

The hardness of ADI280 was 45 HRC, likewise CADI 360, while that of CADI280 was the highest with 50 HRC. These results also show that the CADI360 matrix with 404 HV_{300} was significantly softer than that of CADI280 with 491 HV_{300}, and ADI280 with 510 HV_{300}, but had the same bulk hardness as ADI280 due to the reinforcement provided by the carbides with about 1000 HV.

Table 5: Hardness and Young modulus by nano indentation tests.

Identif.	Hardness (HVeq)	Std. Dev	Young modulus E (GPa)	Std. Dev
ADI280	860	20	240	13

CADI280	888	17	246	10
CADI360	696	48	243	11
Carbide	1224	283	241	30
Graphite	-	-	44	28

Table 6: Bulk and matrix hardness.

Identif.	Bulk (HRC)	Std. Dev	Matrix (HV_{300})	Std. Dev
ADI280	45	0.41	510	55
CADI280	50	0.98	491	33
CADI360	45	0.75	404	21

3.2 RCF behavior

The applied contact pressure, p_0, should be high enough to cause the micro-asperities contact and therefore material micro plasticity and degradation, but not to cause material bulk damage or material build up along the edges of the rolling tracks. Otherwise, this would change contact geometry and contact pressure distribution and thus invalidate the tests. The presence of material build up was verified by using a stylus profilometer in all tests. The characteristic profiles for the different material variants after and before tests, when compared, Fig. 10, show that there was no material build up in any sample and also plasticity was minimal. Also seen from the rolling track depth of about a thousand times smaller than the rolling track width (RTW).

The characteristic contact fatigue failures or spalls observed in each material variant are shown in Fig. 11. The spalls were similar in aspect and dimensions, indicating that the different samples suffered a similar failure mechanism, with surface-initiated cracks propagating underneath the rolling track up to the point where the spall is formed.

Eight tests were carried out for each material variant in order to obtain sufficient datum for the Weibull analysis plots, as shown in Fig. 12, where Failure Probability is plotted against the number of Load Cycles. The characteristic Weibull parameters are summarized in Table 7.

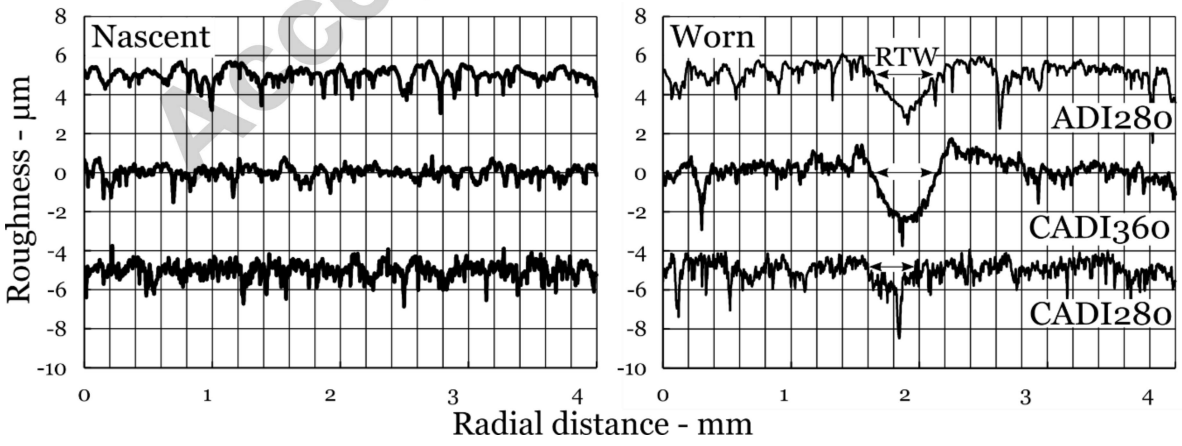

Fig. 10: Stylus profiles of rolling tracks, before and after tests showing deformation and wear for the different material variants and corresponding hardness.

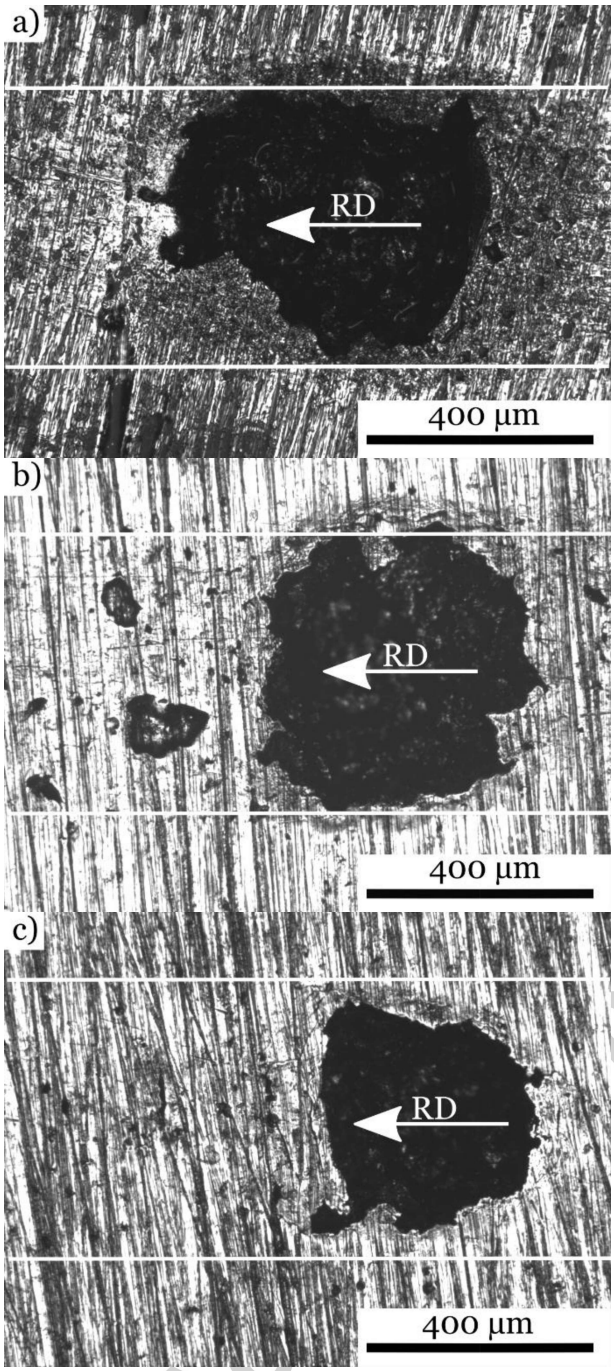

Fig. 11: Characteristic spalls of the different material variants, a) ADI280, b) CADI360, c) CADI280. Rolling Direction (RD) is from right to left. The rolling track width is between the white lines leaving the untested sample surface outside the white lines for comparison.

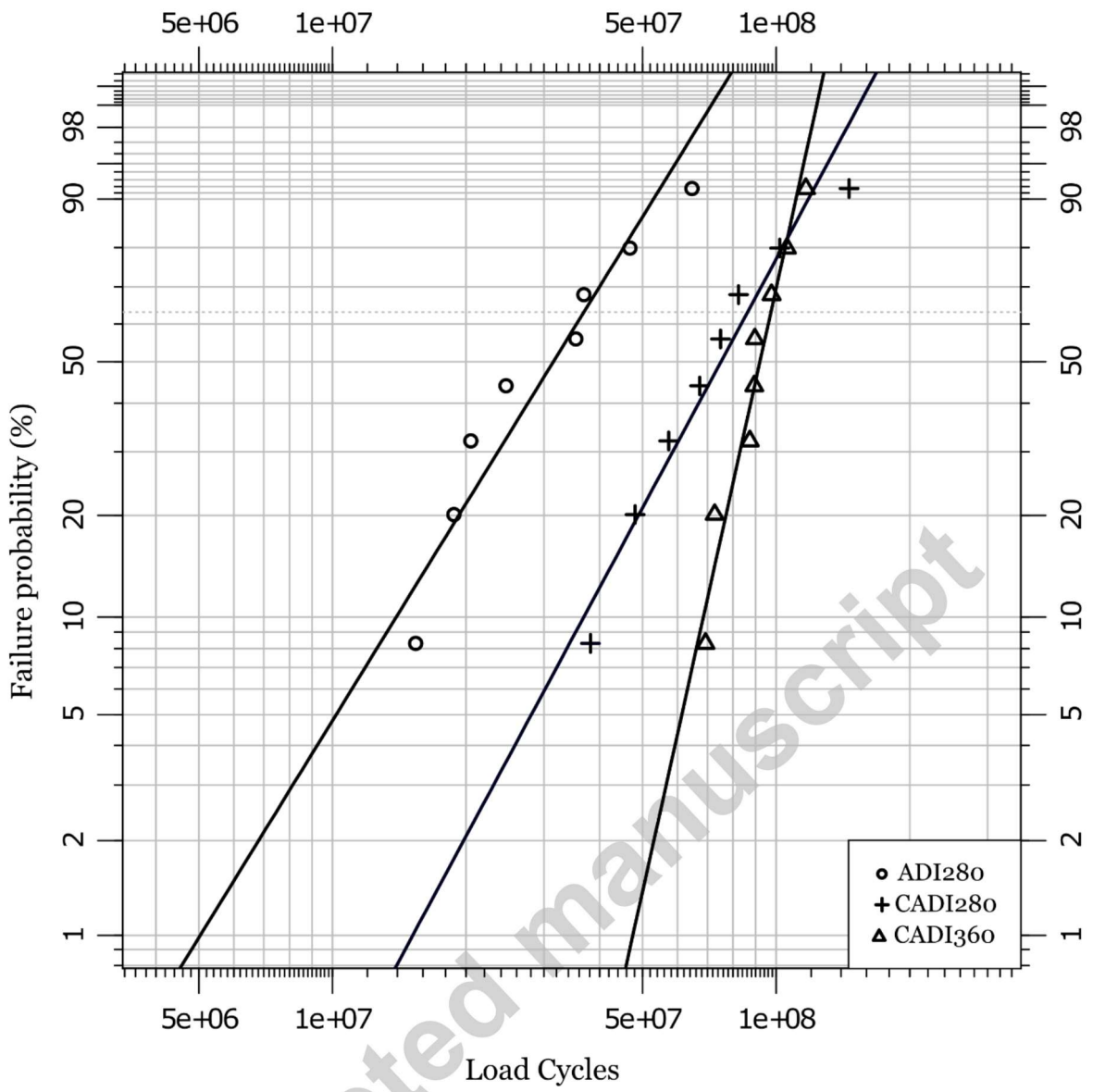

Fig. 12: RCF failure probability vs. number of load cycles for ADI280, CADI360 and CADI280. Testing conditions: $p_0 \approx 1.8$ GPa, calculated $2a = 370$ μm.

Table 7: Summary of material characteristics and Weibull parameters.

Identif.	λ	HRC	NC	NS - μm	% Grap	% Carb	L_{50}(*)	η ($L_{63.3}$) (*)	ß	R^2
ADI280	1.89	45	320	18	8.6	0	31.48	36.89	2.31	0,92
CADI360	1.91	45	193	21	6.1	6.4	91.95	97.35	6.42	0,95
CADI280	1.84	50	193	21	6.1	6.4	75.14	86.29	2.65	0,95

(*) L_{50} and η units are millions of load cycles (x10^6 load cycles)

3.3 Discussion

When comparing ADI280 and CADI280, both materials had similar metallic matrix, with 510 HV and 491 HV, respectively, but the latter was reinforced with ~6.4 % carbides, being the main difference between them, and a bulk hardness of 45 HRC for ADI280 and 50 HRC for CADI280. This higher hardness of CADI280 improved its load carrying capacity, which in turn promoted rolling tracks profiles, Fig. 10, showing that CADI280 was less sensitive to the contact pressure.

The RCF failure mechanism is a process intimately related with micro-plasticity accumulation and therefore it is expected a strong dependency with the materials hardness. By analyzing the RCF test results it is observed that the CADI280 had the highest hardness (50 HRC) and had a RCF L_{50} life 2.4 times higher than that of the reference material ADI280 (45 HRC), but in the case of the CADI360 variant, this one had the same hardness as the reference material but an L_{50} life 2.9 times higher. By comparing both CADI variants, even though CADI360 was softer than CADI280 had an L_{50} life 1.2 times higher.

Then, it seems that while hardness is a dominant property in RCF for homogeneous materials, its relative importance is lower for heterogeneous materials where other microstructural characteristics may become important. For example, inclusions frequently act as crack nucleation points in fatigue [8, 9] by affecting the local stress concentrations due to the difference in its properties compared to the matrix [10, 11]. In this sense, taking into account one of the microstructural features as the NC, ADI samples had 1.7 times the CADI NC and significantly lower L_{50} life, opposite to other authors observations on ADI with increasing NC, but at the same time decreasing NS [12]. In the present work when shifting from ADI to CADI the nodule count decreased from 320 to 193 nod/mm^2 but the nodule size remained about the same decreasing from 21 to 18 μm.

Since the first works on the study of crack initiation and propagation stages [13, 14] many work has been done to understand RCF failure in homogeneous materials like quenched and tempered steels. However, in recent years there has been hard work on understanding the failure mechanism in materials with heterogeneous structures comprising both compliant and/or stiff inclusions or local variations in the mechanical properties [8,9,10,11,15].

In this sense, CADI samples showed lower NC with similar NS and this was reflected in 29.1 % lower graphite content of CADI samples as part of the carbon content was consumed by carbides. Stiff inclusions (carbides) and compliant inclusions (graphite) increase the equivalent stress state, but compliant inclusions bring more severe stress concentrations than stiff ones [15] and then, the difference between CADI360 and ADI280 Weibull plots can be analyzed taking this into account. Moreover, the modulus of elasticity of carbides (Table 5) resulted to be almost equal to that of the metallic matrix and therefore had a small influence on the stress field in the vicinity of the particle. On the other side, the elasticity modulus of graphite resulted almost 5 times lower and hence had a strong influence on the stress field near the nodule. Both samples had similar hardness and, letting aside the presence of carbides, they had the same type of defect, graphite nodules of same average size. According to the work of N. Raje et al. [16], the L_{50} life and the Weibull slope (β) can be related to the difference found in the number of defects, in the

present work the amount of graphite nodules or NC. They [16] found a lower Weibull slope and shorter RCF life while increasing the number of defects.

When considering the crack nucleation stage of the failure process, the nodules open to the surface act as defects increasing the contact stress particularly at the edges of the feature [15, 17]. In addition, nodules at or close to the surface make these materials to have low sensitivity to extrinsic defects as indentations or machining marks, leading to a low resistance to spall nucleation [18]. Considering fatigue as a probabilistic failure and also that all the material variants analyzed had similar NS, is the NC what dominates the probability for crack initiation and ultimately the RCF life.

Despite its lower hardness, the RCF L_{50} life of the CADI360 samples was 1.2 times higher than that of CADI280. In this respect, it must be considered that under ideal RCF conditions most of the life up to the failure event is consumed by the nucleation stage, either in bending fatigue or in RCF. Nevertheless, under non-ideal RCF conditions (when the lubrication regime promote the contact of micro-asperities) the nucleation stage is greatly decreased, and at the same time, the propagation stage is expected to play a significant impact in the overall RCF life [19].

In this respect, when analyzing the crack propagation process the matrix microstructure became important. In these tests the CADI360 with feathery-type ferrite outperforms the CADI280 with its acicular ferrite. This performance is consistent with the work of Tayanc [20] where feathery type ferrite corresponding to upper ausferrite resulted in higher fatigue strength than acicular ferrite. In this work, this response could be attributed to the difference in the retained austenite content with 50.1 % for CADI360 and 37 % for CADI280, since austenite not only has a high deformation capacity but also transforms into martensite assisted by the stress and strain field at the crack tip, [21]. This behavior has been observed in ADI [22] and it is supposed that the ~3 to 4 % volume change associated with this transformation increase the residual compressive stress and decrease the crack propagation rate.

Based on the current work the RCF resistance of CADI depends on the balance of the different phases present in its microstructure, mainly carbides, graphite and the characteristics of the ausferritic matrix. Future work should include testing of CADI with different carbide/graphite balance, in order to determine the amount with the better response under RCF conditions.

4 Conclusions

The RCF behavior of CADI with two different heat treatments was studied and compared to that of an ADI. Tests were performed in a flat washer type machine under conditions leading to a mixed lubrication regime. Main conclusions are:

- Heterogeneous materials under RCF perform in a different way than homogeneous materials and different material properties (hardness, toughness and others) may change its relative importance.
- In general, CADI performed better than ADI under RCF conditions. The RCF life of CADI was higher than that of ADI by factors of 2.9 for CADI360 and 2.4 for CADI280. This response is attributed to the fact that the CADI microstructure replaces part of the ADI nodules by carbides, thus decreasing the nodule count which work as preferential sites for crack nucleation.

- Both compliant and stiff inclusions have detrimental effects on RCF performance
- Soft or compliant inclusions as micro-voids and graphite are very harmful for RCF life and their presence at or close to the surface must be controlled, if possible
- Stiff inclusions (carbide), even though detrimental for RCF performance when comparing to homogeneous materials, are less harmful than the compliant ones (graphite) in CADI. Therefore, an optimal ratio between stiff and compliant inclusions (carbides and graphite in CADI) is expected to maximize its RCF life.
- Carbide reinforcement increased hardness and load carrying capacity.
- These promising results opens new potential application areas for CADI.
- Future research is required to fully understand the reinforcement mechanism of carbides in ADI and the main microstructural characteristics influencing its RCF life.

Funding

This work was supported by The National Scientific and Technical Research Council of Argentina (CONICET) (PIP 1122015 0100756 CO).

References

[1] L. Magalhães, J. Seabra, Wear and scuffing of austempered ductile iron gears, Wear 215 (1998) 237-246.
[2] R. Dommarco, I. Galarreta, H. Ortiz, P. David, G. Maglieri, The use of ductile iron for wheel loader bucket tips, Wear 249 (2001) 101-108.
[3] S. Laino, J. Sikora, R. Dommarco, Development of wear resistant carbidic austempered ductile iron (CADI), Wear 265 (2008) 1-7.
[4] K. Hayrynen, K. Brandenberg, Carbidic Austempered Ductile Iron (CADI) – The New Wear Material, Transactions of the American Foundry Society 111, Paper No 03-088 (2003) 845-850.
[5] C. F. Jatczac et al., Retained Austenite and Its Measurement by X-Ray Diffraction, SAE Special Publication 453 (1980).
[6] W. C. Oliver, G. M. Pharr, An improved technique for determining hardness and elastic modulus using load and displacement sensing indentation experiments, Journal of Materials Research 7 (6) (1992) 1564-1583.
[7] B.J. Hamrock, D.Dowson, Isothermal elastohydrodynamic lubrication of point contacts: Part III—Fully flooded results, Journal of Lubrication Technology 99 (1977) 264-276.
[8] K. Nishioka, On the Effect of Inclusion Upon the Fatigue Strength, journal of the Japan Society for Testing Materials 6 (1957) 382–385.
[9] Y. Murakami, S. Kodama, S. Konuma, Quantitative Evaluation of Effects of Non-Metallic Inclusions on Fatigue Strength of High Strength Steels. I: Basic Fatigue Mechanism and Evaluation of Correlation Between the Fatigue Fracture Stress and the Size and Location of Non-Metallic Inclusions, International Journal of Fatigue 11 (5) (1989) 291–298.
[10] H. J. Bohmer, Rolling Contact Fatigue, Research—A Basis for Products of the Future, FAG Publication No. WL40205EA (1993) 37–45.
[11] H. J. Bohmer, A New Approach to Determine the Effect of Nonmetallic Inclusions on Material Behavior in Rolling Contact, Creative Use of Bearing Steels, ASTM STP No. 1195, J. J. C. Hoo, ed. (1993) 211–221.
[12] N. Rebasa, R. Dommarco, J. Sikora, Wear resistance of high nodule count ductile iron, Wear 253 (2002) 855-861.
[13] S. Way, Pitting due to rolling contact, Journal of Applied Mechanics 57 (1935) 49–58.
[14] A. F. Bower, The influence of crack face friction and trapped fluid on surface initiated rolling contact fatigue cracks, Journal of Tribology 110 (1988) 704-711.

[15] W. Yang, Y. Huang, Q. Zhou, J. Wang, X. Jin, L. M. Keer, Parametric study on stressed volume and its application to the quantification of rolling contact fatigue performance of heterogeneous material, Tribology International 107(2017) 221-232.
[16] N. N. Raje, F. Sadeghi, R. G. Rateick Jr., M. R. Hoeprich, A Numerical Model for Life Scatter in Rolling Element Bearings, ASME J. Tribol., 130 (1) (2008) 011011.
[17] V. Gupta, G. Hahn, P. Bastias, C. Rubin, Influence of indent geometry on repeated two-dimensional rolling contact, Journal of Tribology 117 (1995) 655-659.
[18] R. Dommarco, P. Bastias, H. Dall'o, G. Hahn, C. Rubin, Rolling Contact Fatigue (RCF) resistance of Austempered Ductile Iron (ADI), Wear 221 (1998) 69-74.
[19] P. Rycerz, A. Olver, A. Kadiric, Propagation of surface initiated rolling contact fatigue cracks in bearing steel, International Journal of Fatigue 97 (2017) 29-38.
[20] M. Tayanc, K. Aztekin, A. Bayram, The effect of matrix structure on the fatigue behavior of austempered ductile iron, Materials & Design 28 (2007) 797-803.
[21] A. P. Voskamp, Material Response to Rolling Contact Loading, Journal of Tribology. 107 (1985) 359-366.
[22] M. Johansson, Austenite-Bainitic Ductile Iron, AFS Transactions 85 (1977) 117-122.

Highlights

- Heterogeneous materials under RCF perform different than homogeneous materials.
- In general, CADI performed better than ADI under RCF conditions.
- Compliant inclusions as micro-voids and graphite are very harmful for RCF life.
- Carbide inclusions are less harmful than graphite for RCF performance.
- Carbide reinforcement increased hardness and load carrying capacity.